INL/CON-16-38142
PREPRINT

Simulation of Hydraulic and Natural Fracture Interaction Using a Coupled DFN-DEM Model

50th U.S. Rock Mechanics/Geomechanics Symposium

J. Zhou and H. Huang
(Idaho National Laboratory)

M. Deo
(University of Utah)

March 2016

The INL is a
U.S. Department of Energy
National Laboratory
operated by
Battelle Energy Alliance

Simulation of Hydraulic and Natural Fracture Interaction Using a Coupled DFN-DEM Model

Zhou, J.
Idaho National Laboratory, Idaho Falls, Idaho, USA
Huang, H
Idaho National Laboratory, Idaho Falls, Idaho, USA
Deo, M.
Department of Chemical Engineering, the University of Utah, Salt Lake City, Utah, USA

ABSTRACT: The presence of natural fractures will usually result in a complex fracture network due to the interactions between hydraulic and natural fracture. The reactivation of natural fractures can generally provide additional flow paths from formation to wellbore which play a crucial role in improving the hydrocarbon recovery in these ultra-low permeability reservoir. Thus, accurate description of the geometry of discrete fractures and bedding is highly desired for accurate flow and production predictions. Compared to conventional continuum models that implicitly represent the discrete feature, Discrete Fracture Network (DFN) models could realistically model the connectivity of discontinuities at both reservoir scale and well scale. In this work, a new hybrid numerical model that couples Discrete Fracture Network (DFN) and Dual-Lattice Discrete Element Method (DL-DEM) is proposed to investigate the interaction between hydraulic fracture and natural fractures. Based on the proposed model, the effects of natural fracture orientation, density and injection properties on hydraulic-natural fractures interaction are investigated.

1. INTRODUCTION

It has been widely inferred from numerical modelling[1], [2], laboratory experiments[3], [4] and microseismic monitoring [5], [6] that hydraulically-induced fractures in shale reservoirs often deviate from a simplistic bi-winged fracture geometry. Complex fracture networks generically occur. Some complexity may be caused by stress shadowing resulting from multiple hydraulic fractures interfering during propagation or by interaction with pre-existing natural fractures. According to well logging data, it has been widely accepted that in reservoir with ultra-low permeability such as Barnett, the natural fractures are widely distributed [7]–[9] which may result in hydraulic fractures branching and merging at the Hydraulic Fracture (HF) – Natural Fractures (NF) interface and consequently lead to the creation of the complex fracture network. Therefore, understanding the interaction between hydraulic fracture and natural fracture is important for quantifying the conductive fracture network's extent and for optimizing well completion strategies.

The fracture interactions depend on a variety of parameters including the in-situ stress magnitude and orientation, formation mechanical properties and degree of anisotropy, the existence of so-called dry zone or process zone, the natural fracture's mechanical and fluid transport properties and orientations, as well as treatment characteristics such as fracturing fluid viscosity, local injection rate, and proppant concentration. A number of methods have been used and attempted to understand the combined effects of these parameters on the morphology of the generated fracture network [10]–[13].

Extensive experimental researches have been conducted to investigate the HF-NF interaction and effects of different parameters. Warpinski [3], Teufel [14] and Blanton [15] used hydrostone and sandstone to examine the effects of interface angles and stress conditions on the facture pattern. This revealed that a hydraulic fracture tends to arrest and divert into natural fracture when there is a small stress difference and a small angular variation between the propagating hydraulic fracture and discontinuity it approaches to. Based on laboratory results, analytical developments and numerical insights criteria have been developed to rationalize HF-NF intercepting behavior, providing a basis for projecting experimental results to field scale scenarios.

Considering the expense and upscaling difficulties related to acquiring a core sample representative of the heterogeneities in an entire reservoir, microseismic data have been used to predict and map the induced fracture network in naturally fractured reservoirs at the reservoir

scale. Microseismity is often characterized as a diffuse cloud of events surrounding hydraulically-related fractures and mechanical domain deformation. Shear failure events are commonly detected although tensile failure events are also likely to be ubiquitous. The resolution of these data is currently insufficient to precisely describe the hydraulically-induced, opened or reactivated features. Moreover, neither experimental nor microseismic data are able to predict the detailed growth and interaction behavior of hydraulic fractures.

Numerical modeling provides another powerful avenue to examine the reactivation of natural fractures. The displacement discontinuity method (DDM) is commonly used in hydraulic fracture modeling for its efficiency and accuracy. Kresse et.al. [16] proposed a semi-analytical fracture modeling platform (UFM, OpenT) that includes both the fracture interaction and flow rate effect in the simulation. Also based on the DDM concept, the OpenT model can capture the influences of natural fracture orientation, natural fracture friction coefficient and in-situ stress on hydraulic fracture-natural fracture interactions. Wu and Olson [17] developed a simplified 3D DDM model to simulate the hydraulic fracture-natural fracture interaction and investigated the effect of natural fracture length, in-situ stress and relative angle on the induced fracture pattern. Two different crossing criteria were used to predict the interaction behavior at the frictional interface for fully cemented (welded) natural fractures. Huang et.al. [18] combined geomechanics simulations based on DDM with feedback from microseismic data to calibrate a numerical model and assess hydraulic fracturing performance for a Barnett shale stimulation. Such DDM approaches can simulate the complex interaction between hydraulic and natural fractures, but with the strict assumption of formation homogeneity. There are numerous other methodologies for simulating fracture propagation. For example, Rahman and Rahman [19] used a finite element method to simulate the fracture propagation behavior in poroelastic environments. Dahi-Taleghani and Olson [20] used Extended Finite Element Method (XFEM) model to simulate the hydraulic fracture interaction with natural fracture. The XFEM can handle heterogeneous reservoir and complex boundary conditions without the requirement of grid remeshing but with a heavy computational load.

In this paper, a fully coupling geomechanics and flow hydraulic fracture simulator, which is based on dual-lattice discrete element method, is used to predict generation of a complicated fracture network in the presence of pre-existing natural fractures. Unlike the tradition way of modeling the natural fracture by breaking or weakening particle bonds in discrete element method (DEM), a new inherent friction free algorithm is proposed to eliminate the natural fracture interface friction brought by particle displacements. The effects of natural fracture orientation, density and injection properties on hydraulic-natural fractures interaction are investigated. Both deterministic and stochastic discrete fractures are taken into consideration in the coupling simulation

2. METHODOLOTY

2.1. DEM Modeling

The Dual-Lattice Discrete Element Method (DL-DEM) is based on the discrete element method proposed by Cundall and Strack in 1979 [21]. The figure 1 gives the schematic plot of Dual-Lattice concept. In this model, rock is represented by a collection of randomly generated, nonuniform-sized circular rigid particles that may be joined by elastic beams. Those connected bonds with varying properties (normal force constant and critical strain) form the first type of lattice – DEM lattice (Figure 1 (a), blue lattice). The size and distribution of rock particles are arbitrary, but all particles will behave homogeneously and isotropically at the macroscale. Based on the DEM lattice, a conjugate flow lattice (Figure 1(b), red lattice) is constructed, which explicitly represents the possible flow path of injection fluid.

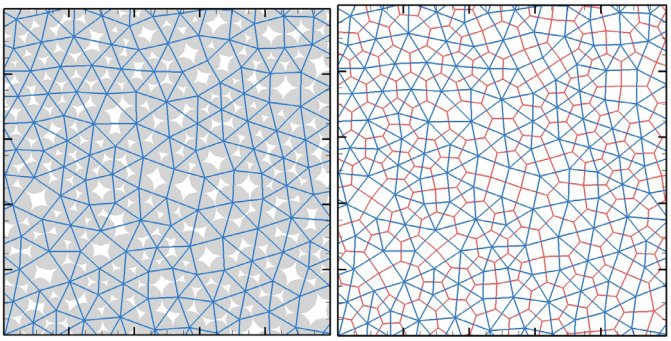

(a) (b)

Fig. 1. The concept of Dual-Lattice DEM model.

These beams can sustain with compressive, tensile, shear loading and transmit a bending moment between connected particles. The fracture initiation and propagation is mimicked by beam breakage. This fully coupling rock deformation and fluid flow DL-DEM simulator has shown the ability of predicting the hydraulic fracture propagation and simple hydraulic-natural fractures interactions in the previous publications [22]–[24].

For connected particles i and j, the beam force and moment exerted on a node i by a neighboring node j are given by

$$\vec{F}_{i,j} = k_n\left(d_{i,j} - d_{i,j}^0\right)\vec{n}_{i,j} + k_s\frac{1}{2}\left(\phi_{i,j} + \phi_{j,i}\right)\vec{s}_{i,j} \qquad (1)$$

$$\overrightarrow{M}_{i,j} = k_s d_{i,j}\left[\frac{\Phi}{12}\left(\phi_{i,j} - \phi_{j,i}\right) + \frac{1}{2}\left(\frac{2}{3}\phi_{i,j} + \frac{1}{3}\phi_{j,i}\right)\right] \qquad (2)$$

where $d_{i,j} = \left|\overrightarrow{(x,y)}_i - \overrightarrow{(x,y)}_j\right|$ is the distance between the centers of two DEM nodes *i* and *j*, and $d_{i,j}^0$ is the initial equilibrium (stress free) distance. $\phi_{i,j}$ is the rotational angle in the local frame of the beam. k_n and k_s are the normal and shear force constants which must be calibrated against the desired E_0 and ν. The detailed calibration process has been described in Huang and Mattson [25]. Force-Displacement law is used to determine both the translational and rotational motion of each particle according to its applied force and moment.

Once an external loading is applied (in our problem the loading is imposed by the injection of fluids), an over-relaxation algorithm is used to relax the DEM network to a new state of mechanical equilibrium in which the net forces and moments are zero for all the DEM particles. If a bond, which is treated as beam in our method, satisfies the von Mises failure criterion

$$\tau = \left(\frac{\varepsilon}{\varepsilon_c}\right)^2 + \frac{\max\left(\left|\phi_{i,j}\right|,\left|\phi_{j,i}\right|\right)}{\phi_c} > 1 \qquad (3)$$

it will be irreversibly removed from the DEM network, giving rise to crack initiation and growth. Here ε is the longitudinal strain of the beam, and ε_c is the critical longitudinal tensile strain (the maximum tensile strain that the bond can sustain), and ϕ_c is the critical rotational angle above that the bond will break, even in the absence of tensile strain. Typical values for ε_c and ϕ_c range from 10^{-3} to 10^{-2} for rocks and many other polycrystalline brittle solids. From Eq. (3), it is clear that the beam breakage will occur under the following three conditions: (1) tensile failure only – the beam tensile strain is larger than the critical tensile strain; (2) shear failure only - the beam rotational angle is larger than the critical rotational angle; (3) Combined tensile and shear failure. Therefore, this criterion can simulate both tensile-induced and shear-induced rock failures. For sign convention, we use positive value for tension and negative value for compression.

2.2. Representation of Natural Fractures

In the previous DL-DEM publication [23], the pre-existing discontinuous interfaces/natural fractures are realized by breaking or weakening the bonds between DEM particles along the natural fracture. Based on the knowledge of potential natural fracture locations, which can be obtained from Formation Microseismic Imaging (FMI) logs or core data, a series of DEM bonds are found and linked to explicitly represent the natural fractures. These natural fractures can be either fully opened or partially cemented depending on the type and extent of filling in these fractures. The figure 2 depicts the implementation of natural fracture in the previous DL-DEM simulator (called as Method I). The embedment of natural fracture is realized through the following steps:

1. DEM particles are randomly generated without any prior knowledge about the pre-existing natural fracture.
2. Based on the DEM particles' placement and detailed information of natural fracture, a series of bonds are chosen to represent and match the natural fracture.
3. Break or weaken those bonds by assigning different microproperties to them.

Since the DEM particles are distributed randomly, the natural fractures represented in this way are not perfectly straight and exhibit inherent frictional force. Even if those bonds are totally broken, the simulator cannot predict realistic interface sliding behavior because of the particles distribution and zigzag fracture geometry, illustrated as the red line in figure 2.

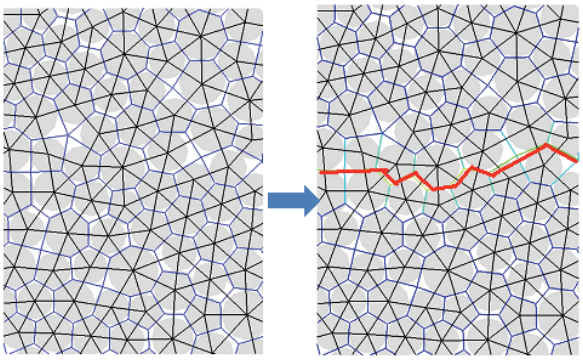

Fig. 2. The implementation of natural fracture in the DL-DEM simulator based on method I.

In order to reduce the roughness of natural fracture interface and remove the inherent friction existed in Method I, we proposed a different implementation strategy in the paper. In this internal friction free algorithm (Method II), all DEM particles used in the simulator can be categorized into two types: particles treated as natural fracture and remaining particles treated as the rock bulk. Instead of generating all particles at one step, the natural fracture particles will be generated and placed prior to the main bulk particles' generation in the Method II. In order to explain the Method II more clearly, an example with single natural fracture is described in Figure 3. Suppose one natural fracture (originates from coordinates (5,5)) exist in the domain with the orientation of 45°, the generation process based on Method II is shown in figure 3, which consists of four critical steps.

At the first step, particles with varying radius are generated and placed with the natural fracture orientation (Figure 3(a), red particles).

After placing all "natural fracture" particles, more rock particles will be generated to fill the domain under the rule of no overlapping between particles (Figure 3(b), grey particles). The particles' diameters satisfy uniform particle size distribution with a predefined average size (D_{ave}) and bounded by D_{min} and D_{max}. In order to ensure dense initial packing, a reduction factor is introduced and multiplied with D_{ave}, D_{min} and D_{max} to shrink the size of particles and increase the total number of created particles. However, because of the non-overlapping rule and the particle diameter constrains, many void interspaces exist in the domain that are not occupied by particles.

At the third step, the generated particles are resized back to original predefined diameter D_{ave} by dividing the reduction factor. A relaxation algorithm is then introduced in this step to adjust the locations of all particles (the particle number will not change) to ensure the sufficiently dense and well-connecting packing pattern. During the relaxation process, all particles are allowed to move until it reaches the maximum allowed step or minimization of overlapping threshold. Particles will exert "pushing force" to their neighboring particles in proportion to their relative distance. The final particles' distribution is shown in figure 3(c). After installation of DEM beams and conjugate flow lattice, the bonds that represent natural fractures will be assigned with different microproperties as shown in figure 3(d).

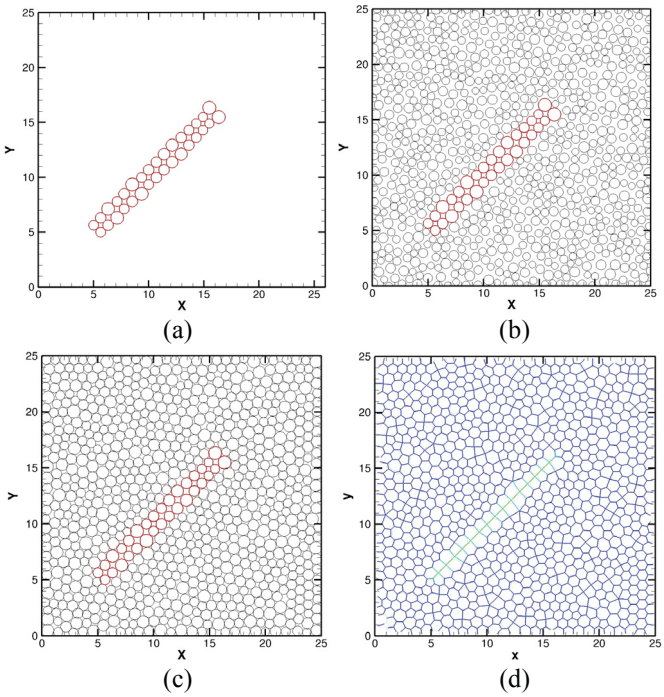

Fig. 3. The procedure of generating natural fracture in the DL-DEM simulator.

With this new NF implementation procedure, the contacting interface of natural fracture will be smooth without any bending, which means that friction coefficient will be more straightforward to control through assignment of microproperties to those bonds.

2.3. DFN Generation

Unconventional formations such as shale gas or tight oil have two special features that differentiate them from conventional reservoirs: 1) Ultra-low permeability at the order of nanodarcy; 2) Pre-existing natural fractures. Compared to conventional continuum models (e.g. dual-porosity model) that implicitly represent the discrete fracture, Discrete Fracture Network (DFN) model is regarded as the most reasonable method that explicitly represents the in-situ joint structure and realistically models the connectivity of discontinuities at both reservoir scale and well scale. A fracture network model should be able to define the basic fracture parameters such as orientation, length, density, etc [26]. For simplicity, the fracture network used in this paper is made of straight lines. In order to generate the fracture network, we need to determine the fracture position, orientation, length and density.

The fracture position is generated according to fractal model, which is based on iterative subdivision cascade process [27], [28]. The principle of this process is recursive fragmentation of a generic shape into n subdomains. The figure 4 gives an example of the first two iterations of this algorithm. In our implementation, at the first iteration (Figure 4 (a)), the domain is separated into four squares with the same size. A probability value (P_1~P_4) is applied to each of the subdomain. Then, at the second iteration (Figure 4(b)), each subdomain is equally divided into four subdomains again. The probabilities (P_1~P_4) are assigned to each of subdomains with different sequences. The number of iteration of the fragmentation process is set to eight in this paper. As a result of this fragmentation process, the fractal probability field is generated. The random locations of natural fractures can be obtained based on this fractal probability field.

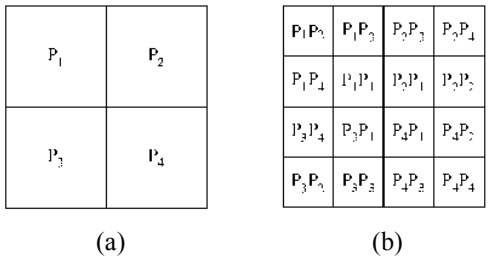

Fig. 4. Illustration of the iterative subdivision cascade process.

Additionally, the fracture length is assumed to satisfy uniform distribution bounded by the smallest and largest fracture length, l_{min} and l_{max}. The fracture orientation also follows the uniform distribution. The DFN embedded into the rock formation is modelled using the internal friction free algorithm proposed in section 2.2.

2.4. *Fluid Flow*

Along with the DEM network, a collection of conjugate flow node is used to explicitly calculate the associated pressure change caused by injection. It is assumed that before the injection, the rock domain does not contain any hydrocarbon. Thus, the fracturing fluid is treated as a single phase, slightly compressible flow. The governing equation for single phase fluid flow in porous media is:

$$\frac{\partial(\varphi\rho_f)}{\partial t} = \nabla\left(\frac{\rho_f k}{\mu}\nabla p\right) + Q \tag{4}$$

where ϕ is the porosity of porous medium, ρ_f is the density of injected fluid, k is the formation permeability, μ is the fluid viscosity, p is the pressure, and Q is the injection rate. Fluid pressure at each conjugate flow node is updated during each time step. And the pressure alteration will exert additional force to the neighboring DEM particles as equivalent body forces. The more detailed descriptions about fluid flow and coupling process can be found in Zhou 2016 [29].

When a bond is broken, a more conductive flow channel will be generated, which connects the two associated fluid nodes in the flow network with the permeability defined as

$$k = \frac{b^2}{12} \tag{5}$$

here b is the aperture of the microfracture (same as the separation distance of the two neighbor DEM particles subject to fracturing). The new permeability will replace the original value in subsequent simulation.

3. NUMERICAL RESULTS

3.1. *Comparison of the two Implementations of Natural Fracture*

In order to illustrate the impact of internal friction brought by the particles placement on the hydraulic and natural fracture interaction, we are firstly going to examine one simple HF-NF interaction case with two different natural fracture implementations (Method I & II). The reservoir is assumed to be homogeneous with the size of 60.96 m (200 *ft*) × 60.96 m (200 *ft*). One natural fracture locates at the center of the domain with the angle α = 80° to the maximum horizontal stress direction. The permeability of NF is 1*md* and the bonds representing the natural fracture are totally broken (cohesion coefficient = 0). A horizontal well with single perforation cluster is located at the bottom of the domain, only one main fracture will be generated through hydraulic fracturing process. The maximum horizontal stress is oriented in the y-direction. The induced fracture geometry is shown in Figure 5.

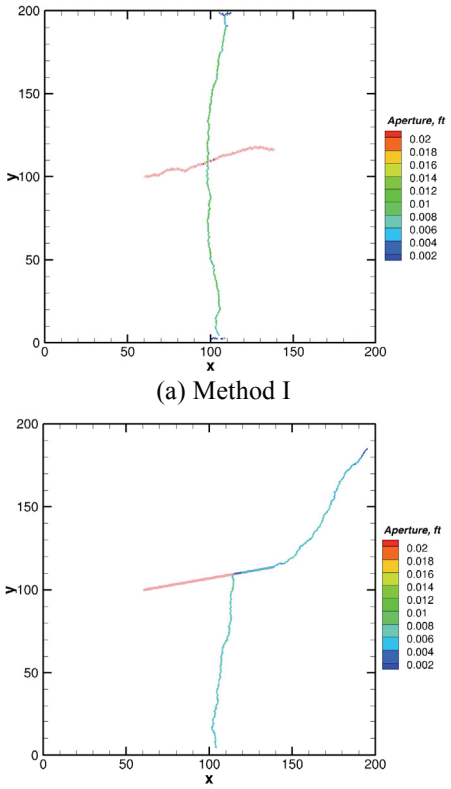

(a) Method I

(b) Method II

Fig. 5. The induced fracture geometry with two different NF implementations.

It can be clearly seen from Figure 5 that with method I algorithm, the natural fracture exhibits some bumpiness and curvature. Under such conditions, the hydraulic fracture directly crosses the natural fracture after HF-NF interception. However, with the method II that is internal friction free algorithm (Figure 4(b)), the hydraulic fracture diverts into the natural fracture and opens it. After reaching to the end of natural fracture, the hydraulic fracture resumes its propagation into the formation with a kink angle, which aligns with the in-situ maximum stress direction.

Even though the approaching angle of the hydraulic fracture is not favorable for natural fracture to open and dilate, the zero cohesion and high permeability of natural fracture makes the interface easier to slide and accepting the injection fluid. Once the inject fluid is accepted by the natural fracture, the increased pressure will drive the opening of natural fracture. This behavior matches with the crossing criterion proposed by Gu and Weng [30]. Therefore, the inherent friction brought by the particle inter-locking can directly affect the HF-NF intercepting behavior. Without considering this friction it will bring bias to the prediction of induced fracture geometry.

3.2. *Sensitivity Analysis*

3.2.1 Reservoir Description

Figure 6 (b) shows the schematic reservoir model used in this section. The reservoir is homogeneous and the size is the same as previous case. The circular DEM particle radius lies from 0.12 *m* (0.4 *ft*) to 0.18 m (0.6 *ft*), and nearly 50000 particles are generated in total. In order to increase the intercepting probabilities, one horizontal well with two perforations clusters is located at the bottom of the domain with the spacing of 20.12 *m* (66 *ft*), one main fracture will generate from each perforation cluster. The total number of natural fractures is 48 with varying location and length. The natural fracture intersection angle (i.e., angle between natural fracture and maximum horizontal stress direction) is 90°. The orientation of all fractures keeps the same. The formation parameters are summarized in Table 1. In order to further illustrate the differences between two natural fracture realizations methods, we also include the natural fracture geometry generated by method I in Figure 6 (a). By comparing those two figures, the interface roughness becomes more severe in multiple natural fractures environment. As mentioned before, those inherent frictions will facilitate the crossing of hydraulic fracture over natural fractures and result in incorrect fracture prediction.

Table 1. Input parameters for the reservoir formation

Parameters	Value
Young's Modulus (GPa)	40
Poisson's Ratio	0.269
Maximum Horizontal Stress (MPa)	48
Formation Permeability (nd)	100
Formation Porosity	0.1
Natural Fracture Orientation	90°
Natural Fracture Cohesion Coefficient	0.4
Natural Fracture Permeability (md)	1

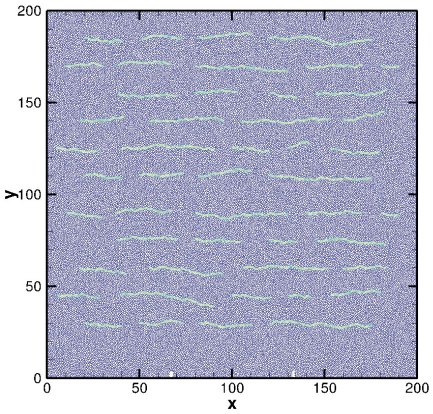

(a) Method I

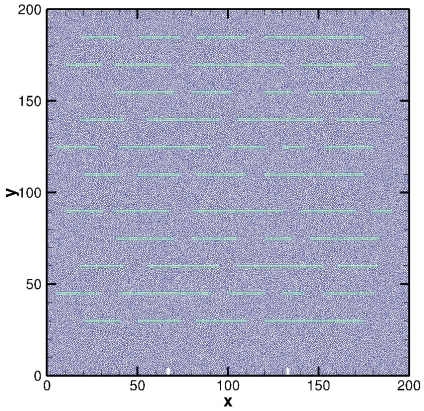

(b) Method II

Fig. 6. The schematic reservoir model with multiple natural fractures.

Since the hydraulic fracturing in the unconventional reservoir is a really complex process, lots of parameters will affect the interaction behavior. In this paper, we are going to examine the impacts of injection properties, orientation and natural fracture density on the induce fracture geometry.

3.2.2 Effect of Injection Viscosity

In the field operation, the fluid used for hydraulic fracturing varies from low-viscosity slickwater to high-viscosity gel. According to experiments and field observations, the injection viscosity greatly impacts the hydraulic and natural fracture interaction. In order to demonstrate the impact of fracturing viscosity on multiple HF/NF interaction, two simulations with different fluid viscosity are used here: 10 *cP* and 800 *cP*. All fractures' cohesion coefficients are 0.4 (Natural Fracture critical strain = Rock formation critical strain × cohesion coefficient) and their permeability is 1 *md*. The far-field in-situ stress ratio is 0.9 ($S_{h,min}/S_{H,max}$ = 0.9). The induced fracture geometries are shown in figure 7.

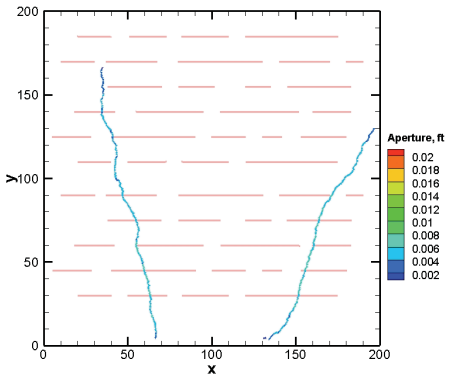

(a) High Viscosity : 800 cP

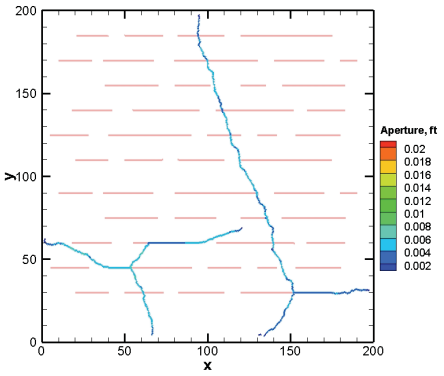

(b) Low Viscosity : 10 cP

Fig. 7. The effect of injection fluid viscosity on HF-NF interactions.

The pressure in the wellbore builds up on injection of the fracturing fluid. Once the pressure at the perforation is large enough to break a particle bond, a microcrack will initialize, coalesce, and propagate further. Therefore, in our case, after injecting for a certain time, two fractures will be growing out of the two perforation clusters. Since multiple natural fractures are existed in the reservoir, the generated fractures will encounter and intercept with multiple natural fractures. Thus the possibility of generating a complex fracture network has also increased.

Figure 7 clearly shows that more viscous fluid tends to cross the natural fractures, whereas low-viscosity fluid will be more easier to penetrate into and open natural fractures. High-viscosity fluid will induce longer fractures with a lower degree of natural fracture reactivation. The low-viscosity fluid injection will facilitate fracture propagation along the natural fractures, which leads to a wider expansion of the fracture network.

In addition, with the low viscous fluid injection, both fractures exhibit branching at the HF-NF interface. For both fractures, the natural fracture is opened by the injecting fluid firstly, and then the "branching" fracture is generated at the contacting point. This branching phenomenon is the result of the competition between dilating favorable viscosity and crossing favorable NF orientation.

3.2.3 Effect of Injection Rate

Besides the injection viscosity, another important injection property, injection rate, is also investigated. In this example, we reduce the injection rate to 0.002 m^2/s (1/3 of the original value). In order to compare with the results in previous section, we run two different simulations with both high and low viscosity. Other operational parameters are the same as the previous example. The induced fracture patterns are shown in Figure 8.

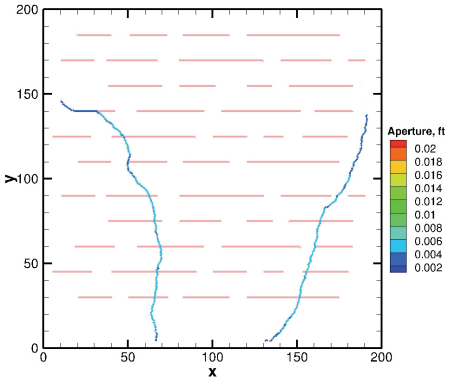

(a) High Viscosity : 800 cP, Low Injection Rate

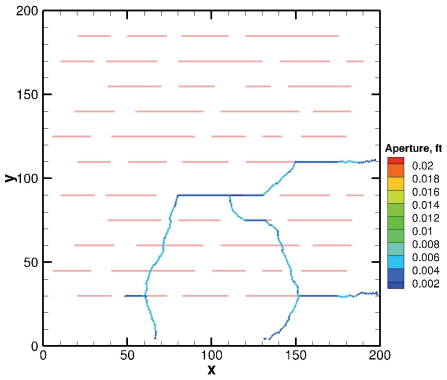

(b) Low Viscosity : 10 cP, Low Injection Rate

Fig. 8. The effect of injection fluid rate on HF-NF interactions.

First, by comparing Figure 8 (a) and Figure 7 (a), the generated fractures are very similar. When the injection fluid viscosity is high, the hydraulic fractures tend to cross the natural fractures with both injection rates. The only difference between the two cases is that the left fracture at low-injection case opens a small natural fracture at the fracture tip.

However, when the viscosity is low, the injection rate will lead to greater impact on the fracture geometry. Instead of propagating across the natural fracture, the hydraulic fractures divert into the natural fracture and change the propagation direction. Finally, it generates a wider but shorter fracture network (Figure 8 (b)).

In summary, the injection fluid with the low injection viscosity or low injection rate will be more easily accepted by the natural fractures, leading to a higher amount of fluid intake into the natural fractures and promoting their reactivation.

3.2.4 Effect of Natural Fracture Orientation

Microseismic data suggest that natural fractures commonly exist in most unconventional reservoirs, especially in shale formations. Natural fractures may be present with multiple orientations within the reservoir, and may not be fully aligned with the current principal in-situ stress direction. The fracture orientation will also affect the HF-NF interaction. Different from case 3.2.2, all fractures' orientation changes from 90^o to 75^o. Two different viscosities are utilized in this case. Both the number and other properties of the pre-existing natural

fractures keep the same. The far-field in-situ stress ratio is still 0.9 ($S_{h,min}/S_{H,max}$ = 0.9). The induced fracture patterns are shown in the figure 9.

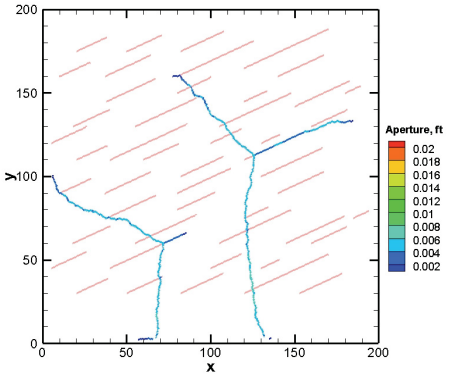

(a) High Viscosity : 800 cP

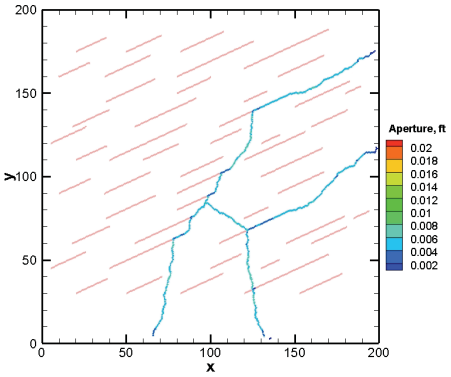

(b) Low Viscosity : 10 cP

Fig. 9. The effect of natural fracture cohesion on HF-NF interactions.

After changing the orientation of the natural fractures, the generated fractures exhibit very different pattern for both high-viscous and low-viscous injection. With more viscous injection, instead of directly crossing multiple natural fractures, the injecting fluid will leak into natural fractures and open it. Same as the previous simulation, the branching effect can be observed at the interface due to the cross-favorable high viscosity. For the low viscosity, the impact of NF orientation becomes more apparent. The hydraulic fractures open most of the encountered natural fracture and change the propagation direction. The final generated fracture pattern exhibits a direction closed to the natural fracture orientation. Therefore, the results indicate that for non-orthogonal interaction, reducing the intercepting angle is more favorable for opening the natural fractures.

Moreover, in all simulation cases, the branching fracture is found to propagate along the direction perpendicular to the dilated natural fracture. The reason is that the opening of the natural fracture will exert additional compressive stress at the neighborhood and reorient the local principal stress direction, which will drive the branching fracture away from the reactivated natural fracture.

3.2.5 Effect of Natural Fracture Density

Besides the natural fracture orientation and injection property, we also investigate the impact of NF density on the HF-NF interactions. At this example, the total number of natural fractures is reduced to 26, almost half of the previous examples. Four different simulations were carried out with different NF orientation and injection viscosity. The induced fracture geometries are summarized in Figure 10.

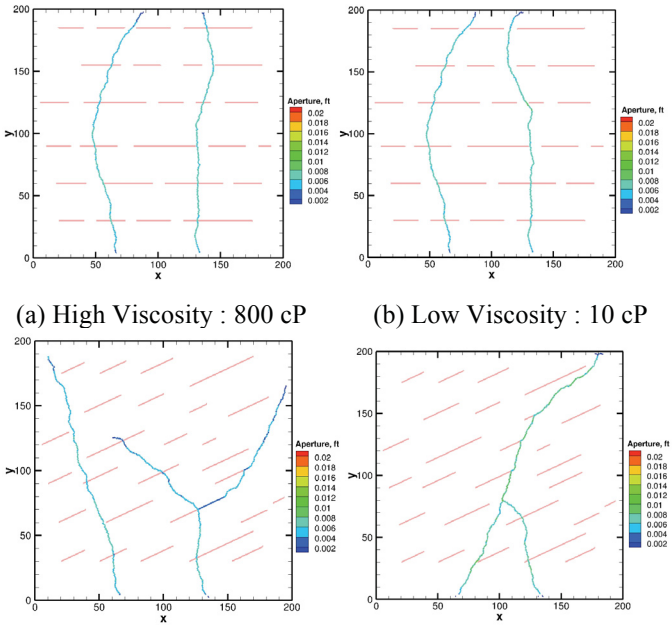

(a) High Viscosity : 800 cP (b) Low Viscosity : 10 cP

(c) High Viscosity : 800 cP (d) Low Viscosity : 10 cP

Fig. 10. The effect of natural fracture density on HF-NF interactions.

With less natural fractures existence, the generated fracture network become much simpler compared with high-density case. The hydraulic fracture will intersect with fewer natural fractures, and thus the possibility of reactivating the NFs and changing the propagation direction is reduced. The natural fracture density will bring larger influence on the induced fracture geometry when the injection viscosity is low.

In addition, compared Figure 9 (a) with (c), Figure 9 (b) with (d), it also verifies that it is easier to reactivate the fracture when the angle of interception is smaller.

3.2.6 Stochastic Natural Fracture

The settings of natural fractures used in all previous examples are generated with predefined locations and orientations. All natural fractures share the same properties without any intersections. However, in the reality, those discontinuities are created by changing of stress mechanism brought by the special geological events, which are generated at different time with different directions. Therefore, natural fractures intersection and hierarchy cannot be ignored in DFN simulations. In this section, multiple fractures with random locations and orientations are generated based on the DFN generation algorithm proposed in section 2.3.

The total number of NF is 53. In order to exclude the disturbances brought by other parameters, the other natural fracture properties, geological parameters and operational parameters are the same as the previous examples. The induced fracture pattern is shown in Figure 11.

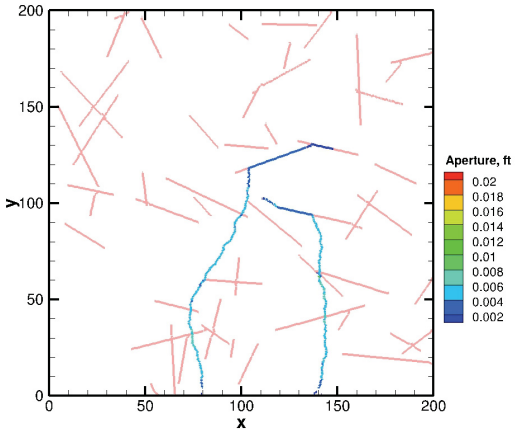

Fig. 11. The induced fracture geometry with stochatic natural fractures.

The red lines in the figure 11 represent generated stochastic natural fractures. It can be observed that the generated fractures pattern is different from the previous simulation results. The fracture propagating direction changes with the orientation of the natural fractures and forms a more unpredictable pattern.

Moreover, since the natural fracture implementation method proposed in this paper is an internal friction free algorithm, the cohesion coefficient is set to be larger than zero to provide additional friction in the previous examples. If the cohesion coefficient is set to zero, the hydraulic fracture will totally deviate into the natural fractures without any branching phenomenon. The results of fully opening natural fracture can be attributed to two reasons: 1) because of the zero cohesion coefficient, the natural fracture is much weaker than the rock formation, and provides the least resistance to fracture opening; 2) the permeability of natural fracture (1 *md*) is much larger than the formation permeability (100 *nd*), the natural fracture also provide a high conductive path for the injection fluid. The induced fracture geometry is shown in Figure 12.

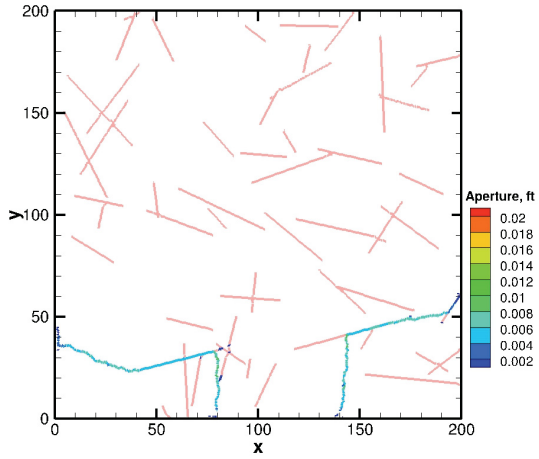

Fig. 12. The induced fracture geometry with zero cohesion coefficient.

4. CONCLUSIONS

The dual-lattice, fully coupled hydro-mechanical hydraulic fracture simulator presented in this paper is able to simulate the propagation of hydraulic fractures in naturally fractured reservoirs. Moreover, a new method of embedding the natural fracture into unconventional reservoir is proposed. With this method, the inherent friction brought by the particle placement and interface roughness is reduced. Based on this new algorithm, the effects of injection properties, natural fracture orientation and density are examined. The important conclusions are summarized:

(1) Conventional way of incorporating the natural fracture in DEM modeling by breaking or weakening the bonds between DEM particles is problematic, which impedes the fracture crossing and induces the biased predictions.

(2) Lower injection rate or lower injected fluid viscosity leads to more fluid intake into the natural fractures and thus leads to their reactivation.

(3) The stochastic fracture network will lead to a more unpredictable fracture pattern due to the stochastic location and orientation of natural fractures.

(4) Results presented in this study provide guidelines for controlling hydraulic fracture morphology in naturally fractured reservoirs. If a more connected network is desired, it is better to use lower injection rates and fluids with lower viscosity

REFERENCES

[1] H. Ouchi, A. Katiyar, J. T. Foster, and M. . M. Sharma, “A Peridynamics Model for the Propagation

of Hydraulic Fractures in Heterogeneous , Naturally Fractured Reservoirs," in *SPE Hydraulic Fracturing Technology Conference held in The Woodlands, Texas, USA, 3-5 February*, 2015.

[2] B. Damjanac, C. Detournay, and P. A. Cundall, "Three-Dimensional Numerical Model of Hydraulic Fracturing in Fractured Rock Masses," in *Effective and Sustainable Hydraulic Fracturing*, InTech, 2013.

[3] N. R. Warpinski and L. W. Teufel, "Influence of Geologic Discontinuities on Hydraulic Fracture Propagation," *J. Pet. Technol.*, vol. 39, 1987.

[4] R. Suarez-Rivera, B. Connor, J. Kieschnick, and S. Green, "Hydraulic Fracturing Experiments Help Understanding Fracture Branching on Tight Gas Shales," in *41th US Symposium on Rock Mechanics held in Golden, Colorado, USA, 17-21 June*, 2006.

[5] S. C. Williams-Stroud, W. B. Barker, and K. L. Smith, "Induced hydraulic fractures or reactivated natural fractures ? Modeling the response of natural fracture networks to stimulation treatments," in *46th US Rock Mechanics/Geomechanics Symposium held in Chicago,IL, USA, 24-26 June*, 2012.

[6] C. L. Cipolla, M. J. Williams, X. Weng, M. Mack, and S. Maxwell, "Hydraulic Fracture Monitoring to Reservoir Simulation : Maximizing Value," in *SPE Annual Technical Conference and Exhibition, 19-22 September, Florence, Italy*, 2010.

[7] M. Fisher and C. Wright, "Integrating fracture mapping technologies to optimize stimulations in the barnett shale," in *SPE Annual Technical Conference and Exhibition, 29 September-2 October 2002, San Antonio, Texas*, 2002, pp. 1–7.

[8] J. F. W. Gale, R. M. Reed, and J. Holder, "Natural fractures in the Barnett Shale and their importance for hydraulic fracture treatments," in *AAPG Bulletin*, 2007, vol. 91, no. 4, pp. 603–622.

[9] R. Bhide, N. Zhao, J. McLennan, and M. Deo, "Modeling Hydraulic Fracture Propagation In Low Permeability Reservoirs," in *46th US Rock Mechanics/ Geomechanics Symposium,held in Chicago,IL, USA, 24-27 June*, 2012.

[10] F. Zhang, N. Nagel, and F. Sheibani, "Evaluation of Hydraulic Fractures Crossing Natural Fractures at High Angles Using a Hybrid Discrete-Continuum Model," in *48th US Rock Mechanics/Geomechanics Symposium held in Minneapolis, MN, USA, 1-4 June*, 2014.

[11] X. Weng, O. Kresse, C. E. Cohen, R. Wu, and H. Gu, "Modeling of Hydraulic Fracture Network Propagation in a Naturally Fractured Formation," in *SPE 140253 Hydraulic Fracturing Technology Conference, Woodlands, Texas, USA, 24-26 January*, 2011, vol. i.

[12] I. Gil, N. Nagel, M. Sanchez-nagel, and B. Damjanac, "The Effect of Operational Parameters on Hydraulic Fracture Propagation in Naturally Fractured Reservoirs – Getting Control of the Fracture Optimization Process," in *45th US Rock Mechanics/Geomechanics Symposium, San Francisco, CA, USA, 26-29 June*, 2011, no. 2010.

[13] N. Zhao, J. McLennan, and M. Deo, "Morphology and Growth of Fractures in Unconventional Reservoirs," in *Canadian Unconventional Resources Conference,15-17 November, Calgary*, 2011, pp. 1–14.

[14] L. Teufel and J. Clark, "Hydraulic Fracture Propagation in Layered Rock: Experimental Studies of Fracture Containment," *Soc. Pet. Eng. J.*, vol. 24, no. February, pp. 19–32, 1984.

[15] T. Blanton, "An Experimental Study of Interaction Between Hydraulically Induced and Pre-Existing Fractures," in *Proceedings of SPE Unconventional Gas Recovery Symposium*, 1982, pp. 559–571.

[16] O. Kresse, X. Weng, D. Chuprakov, R. Prioul, and C. Cohen, "Effect of Flow Rate and Viscosity on Complex Fracture Development in UFM Model," in *Effective and Sustainable Hydraulic Fracturing, DOI: 10.5772/56406*, 2013.

[17] K. Wu and J. E. Olson, "Mechanics Analysis of Interaction Between Hydraulic and Natural Fractures in Shale Reservoirs," in *Proceedings of the 2nd Unconventional Resources Technology Conference*, 2014.

[18] J. Huang, R. Safari, K. Burns, I. Geldmacher, U. Mutlu, M. McClure, and S. Jackson, "Natural-Hydraulic Fracture Interaction: Microseismic Observations and Geomechanical Predictions," in *Proceedings of the 2nd Unconventional Resources Technology Conference*, 2014, pp. 1–22.

[19] M. M. Rahman and S. S. Rahman, "Studies of Hydraulic Fracture-Propagation Behavior in Presence of Natural Fractures : Fully Coupled Fractured-Reservoir Modeling in Poroelastic Environments," *Int. J. Geomech.*, no. December, pp. 809–826, 2013.

[20] A. D. Taleghani and J. E. Olson, "How Natural Fractures Could Affect Hydraulic-Fracture Geometry," *SPE J.*, vol. 19, no. February, pp. 161–171, 2013.

[21] P. A. Cundall and O. D. . Strack, "A discrete numerical model for granular assemblies," *Géotechnique*, vol. 29, no. 1, pp. 47–65, 1979.

[22] J. Zhou, H. Huang, and M. Deo, "Simulation of Hydraulic Fracture Propagation in Heterogeneous Reservoir based on a Dual-Lattice Discrete Element Method," in *The 5th International Conference on Coupled Thermo-Hydro-Mechanical-Chemical Process in Geosystems. Salt Lake City, UT, Feb 25-27*, 2015.

[23] J. Zhou, H. Huang, and M. Deo, "Modeling the Interaction Between Hydraulic and Natural Fractures Using Dual-Lattice Discrete Element Method," in *49th US Rock Mechanics / Geomechanics Symposium held*

in San Francisco, CA, USA, 28 June- 1 July, 2015.

[24] J. Zhou, H. Huang, and M. Deo, "A New Physics-Based Modeling of Multiple Non-Planar Hydraulic Fractures Propagation," in *URTeC 2170875. Unconventional Resources Technology Conference held in San Antonio, Texas, USA, 20-22 July*, 2015.

[25] H. Huang and E. Mattson, "Physics-based Modeling of Hydraulic Fracture Propagation And Permeability Evolution of Fracture Network In Shale Gas Formation," in *2014 ARMA 48th US Rock Mechanics/Geomechanics Symposium,Minneapolis, MN, 1-4 June 2014*, 2014.

[26] C. Darcel, O. Bour, P. Davy, and J.-R. de Dreuzy, "Connectivity properties of two-dimensional fracture networks with stochastic fractal correlation," *Water Resour. Res.*, vol. 39, no. 10, pp. 1–13, 2003.

[27] P. Meakin, "Invasion percolation on substrates with correlated disorder," *Phys. A Stat. Mech. its Appl.*, vol. 173, no. 3, pp. 305–324, 1991.

[28] B. Harthong, L. Scholtès, and F. V. Donzé, "Strength characterization of rock masses, using a coupled DEM-DFN model," *Geophys. J. Int.*, vol. 191, no. 2, pp. 467–480, 2012.

[29] J. Zhou, "Hydraulic Fracture Propagation Modeling and Data-based Fracture Identification," the University of Utah, 2016.

[30] H. Gu, X. Weng, J. Lund, M. Mack, U. Ganguly, and R. Suarez-Rivera, "Hydraulic Fracture Crossing Natural Fracture at Nonorthogonal Angles: A Criterion and Its Validation," *SPE Prod. Oper.*, vol. 27, no. 01, 2012.